
Decentralized Transformers with Centralized Aggregation are Sample-Efficient Multi-Agent World Models

Yang Zhang^{1,2*}, Chenjia Bai^{2†}, Bin Zhao^{2,3}, Junchi Yan^{2,4}, Xiu Li¹, Xuelong Li^{2,5}

¹Tsinghua University, ²Shanghai AI Laboratory, ³Northwestern Polytechnical University

⁴School of Artificial Intelligence, Shanghai Jiao Tong University

⁵Institute of Artificial Intelligence (TeleAI), China Telecom

Abstract

Learning a world model for model-free Reinforcement Learning (RL) agents can significantly improve the sample efficiency by learning policies in imagination. However, building a world model for Multi-Agent RL (MARL) can be particularly challenging due to the scalability issue in a centralized architecture arising from a large number of agents, and also the non-stationarity issue in a decentralized architecture stemming from the inter-dependency among agents. To address both challenges, we propose a novel world model for MARL that learns decentralized local dynamics for scalability, combined with a centralized representation aggregation from all agents. We cast the dynamics learning as an auto-regressive sequence modeling problem over discrete tokens by leveraging the expressive Transformer architecture, in order to model complex local dynamics across different agents and provide accurate and consistent long-term imaginations. As the first pioneering Transformer-based world model for multi-agent systems, we introduce a Perceiver Transformer as an effective solution to enable centralized representation aggregation within this context. Results on Starcraft Multi-Agent Challenge (SMAC) show that it outperforms strong model-free approaches and existing model-based methods in both sample efficiency and overall performance.

1 Introduction

Multi-Agent Reinforcement Learning (MARL) has made remarkable progress, which was driven largely by model-free algorithms [31]. However, due to the complexity of multi-agent systems arising from large state-action space and partial observability, such algorithms usually demand extensive interactions to learn coordinative behaviors [16]. A promising solution is building a world model that approximates the environment, which has exhibited its superior sample efficiency compared to model-free approaches in single-agent RL [9, 52, 11, 12, 13, 14]. However, extending the design of world model in single-agent domain to the multi-agent context encounters significant challenges due to the unique biases and characteristics inherent to multi-agent environments.

The challenges primarily stem from two different means for multi-agent dynamics learning: *centralized* and *decentralized*. Learning a world model to approximate the *centralized* dynamics encapsulates the inter-dependency between agents but struggles to be scalable to an increasing number of agents, which leads to the exponential surge in spatial complexity [16, 31]. Conversely, applying a *decentralized* world model to approximating the local dynamics of each agent mitigates the scalability issue

*Work done during an internship at Shanghai AI Lab.

†Correspondence to: Chenjia Bai<baichenjia@pjlab.org.cn>

yet incurs non-stationarity, as unexpected interventions from other agents may occur in each agent’s individual environment [32]. Furthermore, beyond these unique challenges inherent to multi-agent scenarios, existing model-based MARL approaches [47, 5, 48] excessively neglect the fact that the policy learned in imaginations of the world model heavily relies on the quality of imagined trajectories [30]. It thereby necessitates accurate long-term prediction, especially with respect to the non-stationary local dynamics. Inspired by the capability of Transformer [45] in modeling complex sequences and long-term dependency [2, 4, 30], we seek to construct a Transformer-based world model within the multi-agent context for *decentralized* local dynamics together with *centralized* feature aggregation, combining the benefits of two distinctive designs.

In this paper, we introduce MARIE (Multi-Agent auto-Regressive Imagination for Efficient learning), the first Transformer-based multi-agent world model for sample-efficient policy learning. Specifically, **the highlights of this paper are:**

1. To tackle the inherent challenges within the multi-agent context, we build an effective world model via scalable *decentralized* dynamics modeling and essential *centralized* representation aggregating, which mirrors the principle of Centralized Training and Decentralized Execution.
2. To enable accurate and consistent long-term imaginations from the non-stationary local dynamics, we cast the *decentralized* dynamics learning as sequence modeling over discrete tokens by leveraging highly expressive Transformer architecture as the backbone. In particular, we successfully present the first Transformer-based world model for multi-agent systems.
3. While it remains open for how to effectively enable *centralized* representation with the Transformer as the backbone, we achieve it by innovatively introducing a Perceiver Transformer [19] for efficient global information aggregation across all agents.
4. Experiments on the Starcraft Multi-Agent Challenge (SMAC) [38] benchmark in low data regime show MARIE outperforms both model-free and existing model-based MARL methods w.r.t. both sample efficiency and overall performance and demonstrate the effectiveness of MARIE.

2 Related Works and Preliminaries

Multi-Agent Reinforcement Learning. In a model-free setting, a typical approach for cooperative MARL is centralized training and decentralized execution (CTDE), which tackles the scalability and non-stationarity issues in MARL. During the training phase, it leverages global information to facilitate agents’ policy learning; while during the execution phase, it blinds itself and has only access to the partial observation around each agent for multi-agent decision-making. Model-free MARL methods with this paradigm can be divided into 2 categories: value-based [42, 35, 41, 46] and policy-based [28, 7, 18, 37, 27, 25, 33, 49, 51, 50]. In contrast to model-free approaches, model-based MARL algorithms remain fairly understudied. MAMBPO [47] incorporates MBPO-style [20] techniques into multi-agent policy learning under the CTDE framework. Tesseract [29] introduces the tensorised Bellman equation and evaluates the Q-value function using Dynamic Programming (DP) together with an estimated environment model. Similar to our setting where agents learn inside of an approximate world model, MAMBA [5] integrates the backbone proposed in DreamerV2 [11] with an attention mechanism across agents to sustain an effective world model in environments with an arbitrary number of agents, which leads to notably superior sample efficiency to existing model-free approaches. In terms of model-based algorithm coupled with planning, MAZero [26] expands the MCTS planning-based Muzero [39] framework to the model-based MARL settings. However, learning-based or planning-based policies in these two approaches are both overly coupled with their world models, downgrading their inference efficiency and further limiting expansion in combinations with other popular model-free approaches.

Learning behaviors within the imagination of world models. The Dyna architecture [43] first emphasizes the utility of an estimated dynamics model in facilitating the training of the value function and policy. Inspired by the cognitive system of human beings, the concept of world model [8] is initially introduced by composing a variational Auto-Encoder (VAE) [24] and a recurrent network to mimic the complete environmental dynamics, then an artificial agent is trained entirely inside the hallucinated imagination generated by the world model. SimPLe [52] shows that a PPO policy [40] learned in a predictive model delivers a super-human performance in Atari domains. Dreamer [9] builds the world model upon a Recurrent State Space Model (RSSM) [10] that combines the deterministic latent state with the stochastic latent state to allow the model to not only capture multiple futures but also remember information over multi-steps. DreamerV2 [11] further demonstrates the advantage

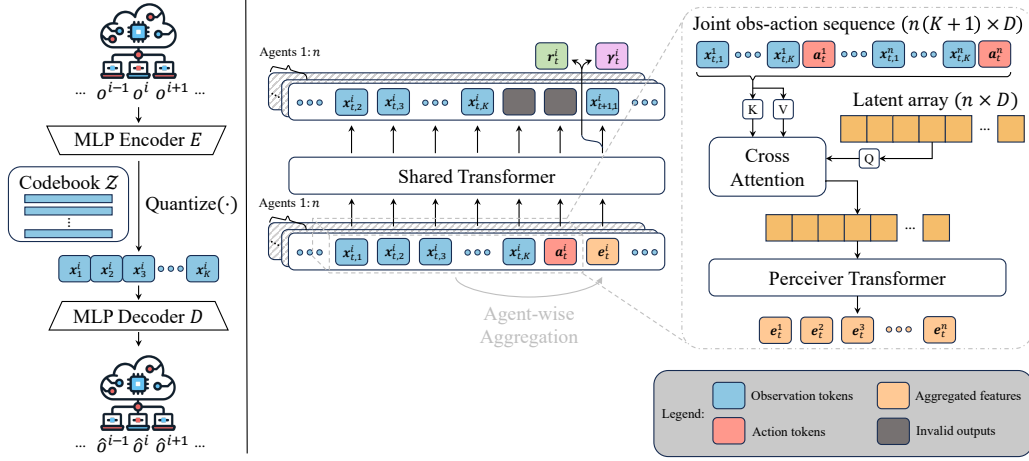


Figure 1: Overview of the proposed world model architecture in MARIE. VQ-VAE (*left*) maps local observations o^i of each agent i into discrete latent codes (x_1^i, \dots, x_K^i) , where (E, D, \mathcal{Z}) is shared across all agents. Together with discrete actions, this process forms local discrete sequences $(\dots, x_{t,1}^i, \dots, x_{t,K}^i, a_t^i, \dots)$ of each agent. Then the Perceiver (*right*) performs aggregation of joint discrete sequences of all agents $(x_{t,1}^1, \dots, x_{t,K}^1, a_t^1, \dots, x_{t,1}^n, \dots, x_{t,K}^n, a_t^n)$ independently at each timestep t , and inserts the aggregated global representations $(e_t^1, e_t^2, \dots, e_t^n)$ into original local discrete sequences respectively. The resulting sequences $(\dots, x_{t,1}^i, \dots, x_{t,K}^i, a_t^i, e_t^i, \dots)$ contain rich information between transitions in local dynamics and are fed into the shared Transformer (*middle*), which learns observation token predictions in an autoregressive manner. Predictions of individual reward r_t^i and discount γ_t^i at timestep t are computed based on all historical sequence $(x_{\leq t,1}^i, \dots, x_{\leq t,K}^i, a_{\leq t}^i, e_{\leq t}^i)$.

of discrete latent states over Gaussian states. For MARL, MAMBA [5] extends DreamerV2 to multi-agent contexts by using RSSM, underscoring the potential of multi-agent learning in the imagination of world models. Recently, motivated by the success of the Transformer [45], TransDreamer [3] and TWM [36] explored variants of DreamerV2, wherein the backbones of the world model were substituted with Transformers. Instead of incorporating deterministic and stochastic latent states, IRIS [30] applies the Transformer to directly modeling sequences of observation tokens and actions of single-agent RL and achieves impressive results on Atari-100k. In contrast, the proposed MARIE concentrates on establishing effective Transformer-based world models in multi-agent contexts with shared dynamics and global representations.

Preliminaries. We focus on fully cooperative multi-agent systems where all agents share a team reward signal. We formulate the system as a decentralized partially observable Markov decision process (Dec-POMDP) [32], which can be described by a tuple $(\mathcal{N}, \mathcal{S}, \mathcal{A}, P, R, \Omega, \mathcal{O}, \gamma)$. $\mathcal{N} = \{1, \dots, n\}$ denotes a set of agents, \mathcal{S} is the finite global state space, $\mathcal{A} = \prod_{i=1}^n \mathcal{A}^i$ is the product of finite actions spaces of all agents, i.e., the joint action space, $P: \mathcal{S} \times \mathcal{A} \times \mathcal{S} \rightarrow [0, 1]$ is the global transition probability function, $R: \mathcal{S} \times \mathcal{A} \rightarrow \mathbb{R}$ is the shared reward function, $\Omega = \prod_{i=1}^n \Omega^i$ is the product of finite observation spaces of all agents, i.e., the joint observation space, $\mathcal{O} = \{\mathcal{O}^i, i \in \mathcal{N}\}$ is the set of observing functions of all agents. $\mathcal{O}^i: \mathcal{S} \rightarrow \Omega^i$ maps global states to the observations for agent i , and γ is the discount factor. Given a global state s_t at timestep t , agent i is restricted to obtaining solely its local observation $o_t^i = \mathcal{O}^i(s_t)$, takes an action a_t^i drawn from its policy $\pi^i(\cdot | o_{\leq t}^i)$ based on the history of its local observations $o_{\leq t}^i$, which together with other agents' actions gives a joint action $\mathbf{a}_t = (a_t^1, \dots, a_t^n) \in \mathcal{A}$, equivalently drawn from a joint policy $\pi(\cdot | \mathbf{o}_{\leq t}) = \prod_{i=1}^n \pi^i(\cdot | o_{\leq t}^i)$. Then the agents receive a shared reward $r_t = R(s_t, \mathbf{a}_t)$, and the environment moves to next state s_{t+1} with probability $P(s_{t+1} | s_t, \mathbf{a}_t)$. The aim of all agents is to learn a joint policy π that maximizes the expected discounted return $J(\pi) = \mathbb{E}_{s_0, \mathbf{a}_0, \dots \sim \pi} [\sum_{t=0}^{\infty} \gamma^t R(s_t, \mathbf{a}_t)]$.

3 Methodologies

Our approach comprises three typical parts: (i) collecting experience by executing the policy, (ii) learning the world model from the collected experience, and (iii) learning the policy via imagination inside the world model. Throughout the process, the historical experiences stored in the replay

buffer are used for training the world model only, while policies are learned from unlimited imagined trajectories from the world model. In the following, we first describe three core components of our world model in §3.1 and §3.2, and give an overview of the proposed world model in Fig. 1. Then we describe the policy-learning process inside the world model in §3.3. The comprehensive details of the model architecture and hyperparameter are provided in §A.

3.1 Discretizing Observation

We consider a trajectory τ^i of agent i consists of T local observations and actions, as

$$\tau^i = (o_1^i, a_1^i, \dots, o_t^i, a_t^i, \dots, o_T^i, a_T^i).$$

To utilize the expressive Transformer architecture, we need to express the trajectory into a discrete token sequence for modeling. Accounting for continuous observations, a prevalent but naive approach for discretization involves discretizing the scalar into one of m fixed-width bins in each dimension independently [21]. However, with a higher dimension of the observation, the Transformer encounters higher computational complexity, which necessitates an approach that uses a discrete codebook of learned representations. To this end, we employ the idea from neural discrete representation learning [44], and learn a Vector Quantised-Variational AutoEncoder (VQ-VAE) to play a role that resembles the tokenizer in Natural Language Processing [4, 2]. The VQ-VAE is composed of an encoder E , a decoder D , and a codebook \mathcal{Z} . We define the discrete codebook $\mathcal{Z} = \{z_j\}_{j=1}^N \subset \mathbb{R}^{n_z}$, where N is the size of the codebook and n_z is the dimension of codes. The encoder E takes an observation $o^i \in \mathbb{R}^{n_{\text{obs}}}$ as input and outputs a K n_z -dimensional latents $\hat{z}^i \in \mathbb{R}^{K \times n_z}$ reshaped from the direct outputs of encoder. Subsequently, the tokens $\{x_k^i\}_{k=1}^K \in \{0, 1, \dots, N-1\}^K$ for representing o^i is obtained by a nearest neighbour look-up using the codebook \mathcal{Z} where $x_k^i = \arg \min_j \|\hat{z}_k^i - z_j\|$. Then the decoder $D : \{0, 1, \dots, N-1\}^K \rightarrow \mathbb{R}^{n_{\text{obs}}}$ converts K tokens back into an reconstructed observation \hat{o}^i . By learning this discrete codebook, we compress the redundant information via a succinct sequence of tokens, which helps improve sequence modeling. See §4.2 for a discussion.

3.2 Modeling Local Dynamics with Global Representations

Here, we consider discrete actions like those in SMAC, and the continuous actions can also be discretized by splitting the value in each dimension into fixed bins [21, 1]. Therefore, a trajectory τ^i of agent i can be treated as a sequence of tokens,

$$\tau^i = (\dots, o_t^i, a_t^i, \dots) = (\dots, x_{t,1}^i, x_{t,2}^i, \dots, x_{t,K}^i, a_t^i, \dots) \quad (1)$$

where $x_{t,j}^i$ is the j -th token of the observation of agent i at timestep t . Given arbitrary sequences of observation and action tokens in Eq. (1), we try to learn over discrete multimodal tokens.

The world model consists of a tokenizer to discrete the local observation, a Transformer to learn the local dynamics, an agent-wise representation aggregation module, and predictors for the reward and discount. The Transformer ϕ predicts the future local observation $\{\hat{x}_{t+1,j}^i\}_{j=1}^K$, the future individual reward \hat{r}_t^i and discount $\hat{\gamma}_t^i$, based on the agent’s individual historical observation-action history $(x_{\leq t}^i, a_{\leq t}^i)$ and aggregated global feature e_t^i of the agent. The modules are shown in Eqs. (2)–(5).

$$\text{Transition: } \hat{x}_{t+1,\cdot}^i \sim p_\phi(\hat{x}_{t+1,\cdot}^i | x_{\leq t,\cdot}^i, a_{\leq t}^i, e_{\leq t}^i) \text{ with } \hat{x}_{t+1,k}^i \sim p_\phi(\hat{x}_{t+1,k}^i | x_{\leq t,\cdot}^i, a_{\leq t}^i, e_{\leq t}^i, x_{t+1,<k}^i) \quad (2)$$

$$\text{Reward: } \hat{r}_t^i \sim p_\phi(\hat{r}_t^i | x_{\leq t,\cdot}^i, a_{\leq t}^i, e_{\leq t}^i) \quad (3)$$

$$\text{Discount: } \hat{\gamma}_t^i \sim p_\phi(\hat{\gamma}_t^i | x_{\leq t,\cdot}^i, a_{\leq t}^i, e_{\leq t}^i) \quad (4)$$

$$\text{Aggregation: } (e_t^1, e_t^2, \dots, e_t^n) = f_\theta(x_{t,1}^1, x_{t,2}^1, \dots, x_{t,K}^1, a_t^1, \dots, x_{t,1}^n, x_{t,2}^n, \dots, x_{t,K}^n, a_t^n) \quad (5)$$

Transition Prediction. In the transition prediction in Eq. (2), the k -th observation token is additionally conditioned on the tokens that were already predicted $x_{t+1,<k}^i \triangleq (x_{t+1,1}^i, x_{t+1,2}^i, \dots, x_{t+1,k-1}^i)$, ensuring the autoregressive token prediction to facilitate modeling over the trajectory sequence.

Discount Prediction. The discount predictor outputs a Bernoulli likelihood and lets us estimate the probability of an individual agent’s episode ending when learning behaviors from model predictions.

Reward Prediction. Since the rewards distribution is widespread and diverse in multi-agent scenarios [38], we discrete the reward and learn a reward predictor via discrete regression [6] instead of a mean-squared error. Specifically, the reward predictor outputs an estimated categorical distribution

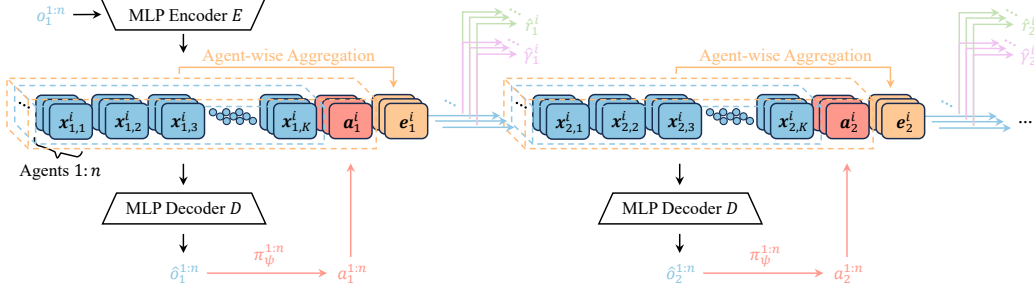


Figure 2: Imagination procedure in MARIE. We unroll the imagination of all agents $\{1, \dots, n\}$ in parallel. Initially, each agent’s observation is derived from a joint observation sampled from a replay buffer. A policy, depicted in red arrows, generates actions based on reconstructed observations. Then, the Perceiver integrates joint actions and observations into global representations from each agent, appending them to each agent’s local sequence. The Transformer then predicts individual rewards and discounts, depicted by green and purple arrows respectively, while generating next observation tokens for each agent in an autoregressive manner, shown by blue arrows. This parallel imagination iterates for H steps. The policies $\pi_\psi^{1:n}$ are exclusively trained using imagined trajectories.

\mathcal{R} over M buckets centered at $\{b_m\}_{m=1}^M$ through the softmax function. The estimated reward is represented as the expected value of this distribution, as

$$\hat{r}_t^i = \mathbb{E} [\mathcal{R}(x_{\leq t}^i, a_{\leq t}^i, e_{\leq t}^i)], \quad \mathcal{R}(x_{\leq t}^i, a_{\leq t}^i, e_{\leq t}^i) = \sum_{m=1}^M p_\phi(b_m | x_{\leq t}^i, a_{\leq t}^i, e_{\leq t}^i) \cdot \delta_{b_m} \quad (6)$$

Then we learn the reward predictor by using the cross-entropy loss function. The target distribution $\mathcal{R}_{\text{tar}} = \sum_{m=1}^M p_m \cdot \delta_{b_m}$ can be calculated via HL-Gauss [6], which performs label smoothing for the target categorical distribution using a Gaussian distribution. The details are given in §B.

Agent-wise Aggregation. Due to the partial environment, the non-stationarity issue stems from the sophisticated agent-wise inter-dependency on local observations generation. To address it, we introduce a Perceiver [19] to perform agent-wise representation aggregation which plays a similar role to communication. To sustain the decentralized manner in transition prediction, we hope every agent can possess its own inner perception of the situations that all agents are in. Nonetheless, with discrete representation for local observation, the observation-action pair of agent i at timestep t is projected into a sequence $(x_{t,1}^i, x_{t,2}^i, \dots, x_{t,K}^i, a_t^i)$ of length $K + 1$. It leads to a sequence of length $n(K + 1)$ that linearly scales with the number of agents, which represents the joint observation-action pair of all agents. Therefore, we choose the Perceiver as the agent-wise representation aggregation module, which excels at dealing with the case that the size of inputs and outputs scales linearly. Equipped with a flexible querying mechanism and self-attention mechanism, the Perceiver aggregates the joint representation sequence $(x_{t,1}^1, x_{t,2}^1, \dots, x_{t,K}^1, a_t^1, \dots, x_{t,1}^n, x_{t,2}^n, \dots, x_{t,K}^n, a_t^n)$ of length $n(K + 1)$ into a sequence of n feature vectors $(e_t^1, e_t^2, \dots, e_t^n)$, where each feature vector serves as an intrinsic global abstraction of the environmental contexts perceived from each agent’s viewpoint.

The world model ϕ is trained with trajectory segments of a fixed horizon H sampled from the replay buffer \mathcal{D} in a self-supervised manner. The transition predictor, discount predictor, and reward predictor are optimized to maximize the log-likelihood of their corresponding targets:

$$\begin{aligned} \mathcal{L}_{\text{Dyn}}(\phi, \theta) = \mathbb{E}_{i \sim \mathcal{N}} \mathbb{E}_{\tau^i \sim \mathcal{D}} \left[\sum_{t=1}^H \underbrace{-\log p_\phi(r_t^i | x_{\leq t}^i, a_{\leq t}^i, e_t^i)}_{\text{reward loss}} - \underbrace{\log p_\phi(\gamma_t^i | x_{\leq t}^i, a_{\leq t}^i, e_t^i)}_{\text{discount loss}} \right. \\ \left. - \left(\sum_{k=1}^K \log p_\phi(x_{t+1,k}^i | x_{\leq t}^i, a_{\leq t}^i, e_t^i, x_{t+1,<k}^i) \right) \right] \quad (7) \end{aligned}$$

$$\text{where } (e_t^1, e_t^2, \dots, e_t^n) = f_\theta(x_{t,1}^1, x_{t,2}^1, \dots, x_{t,K}^1, a_t^1, \dots, x_{t,1}^n, x_{t,2}^n, \dots, x_{t,K}^n, a_t^n), \forall t.$$

We jointly minimize this loss function in Eq. (7) with respect to the model parameters of local dynamics (i.e., ϕ) and global representation (i.e., θ) using the Adam optimizer [23].

3.3 Learning Behaviours in Imagination

We utilize the Actor-Critic framework to learn the behavior of each agent, where the actor and critic are parameterized by ψ and ξ , respectively. In the following, we take agent i as an exemplar case

for clarity and omit the superscript for denoting the index of the agent to avoid potential confusion. Benefited from the shared local dynamics, the local trajectories of all agents are imagined in parallel, as illustrated in Fig. 2. At timestep t , the actor takes a reconstructed observation \hat{o}_t as input, and samples an action $a_t \sim \pi_\psi(a_t|\hat{o}_t)$. The world model then predicts the individual reward \hat{r}_t , individual discount $\hat{\gamma}_t$ and next local observation \hat{o}_{t+1} . Starting from initial observations sampled from the replay buffer, this imagination procedure is rolled out for H steps. To stimulate long-horizon behavior learning, the critic accounts for rewards beyond the fixed imagination horizon and estimates the individual expected return $V_\xi(\hat{o}_t) \simeq \mathbb{E}_{\pi_\psi}[\sum_{l \geq t} \gamma^{l-t} \hat{r}_l]$.

In our approach, we train the actor and critic in a MAPPO-like [49] manner. Unlike other CTDE model-free approaches that require a global oracle state from the environment, we cannot obtain the oracle state from the world model, and only the predicted observations of each agent are available. To approximate the oracle information in critic training, we enhance each agent’s critic with the capability to access the observations of other agents. Since the actor and critic only rely on the reconstructed observations, decoupling from the inner hidden states of the Transformer-based world model, we allow fast inference in the environment without the participation of the world model. It is important for the deployment of policies learned with data-efficient imagination in real-world applications. λ -target in Dreamer [9] is used to updated the value function. The details of behavior learning objectives and algorithmic description of MARIE are presented in §C and §G, respectively.

4 Experiments

We consider the most common benchmark – StarCraftII Multi-Agent Challenge (SMAC) [38] for evaluating our method. To highlight the sample efficiency brought by model-based imagination, we adopt a low data regime that resembles a similar setting in single-agent Atari domain [52].

4.1 Evaluations on SMAC

StarCraftII Multi-Agent Challenge. SMAC [38], a suite of cooperative multi-agent environments based on StarCraft II, consists of a set of StarCraft II scenarios. Each scenario depicts a confrontation between two armies of units, one of which is controlled by the built-in game AI and the other by our algorithm. The initial position, number, and type of units in each army varies from scenario to scenario, as does the presence or absence of elevated or impassable terrain. And the goal is to win the game within the pre-specified time limit. SMAC emphasizes mastering micromanagement techniques across multiple agents to achieve effective coordination and overcome adversaries. This necessitates both sufficient exploration and appropriate credit assignment for each agent’s action. Another notable property of SMAC is that not all actions are accessible during decision-making of each agent, which requires world models to possess an in-depth comprehension of the underlying game mechanics so as to consistently provide valid available action mask estimation within the imagination horizon.

Experimental Setup. We choose 13 representative scenarios from SMAC that includes three levels of difficulty – *Easy*, *Hard*, and *SuperHard*. Specific chosen scenarios can be found in Table 1. In terms of different levels of difficulty, we adopt a similar setting akin to that in [5] and restrict the number of samples from the real environment to 100k for *Easy* scenarios, 200k for *Hard* scenarios and 400k for *SuperHard* scenarios, to establish a low data regime in SMAC. We compare MARIE with three strong model-free baselines – MAPPO [49], QMIX [35] and QPLEX [46], and two strong model-based baselines – MBVD [48] and MAMBA [5] on SMAC benchmark. Specially, as a recently proposed multi-agent variant of DreamerV2 [11], MAMBA achieves state-of-the-art sample efficiency in various SMAC scenarios via learning in imagination. For each random seed, we compute the win rate across 10 evaluation games at fixed intervals of environmental steps.

Main Results. Overall, we find MARIE achieves significantly better sample efficiency and a higher win rate compared with other strong baselines. We report the median win rates over four seeds in Table 1 and provide additional learning curves of several chosen scenarios, shown as Fig. 3. As presented in Table 1 and Fig. 3, MARIE demonstrates superior performance and sample efficiency across almost all scenarios. The improvements in sample efficiency and performance become particularly pronounced with increasing difficulty of scenarios, especially compared to MAMBA that adopts RSSM as the backbone for the world model. We attribute such results to the model capability of the Transformer in local dynamics modeling and global feature aggregation. Benefiting from more powerful strength in modeling sequences, the Transformer-based world model can generate more accurate and consistent imaginations than those relying on the recurrent backbone, which facilitates

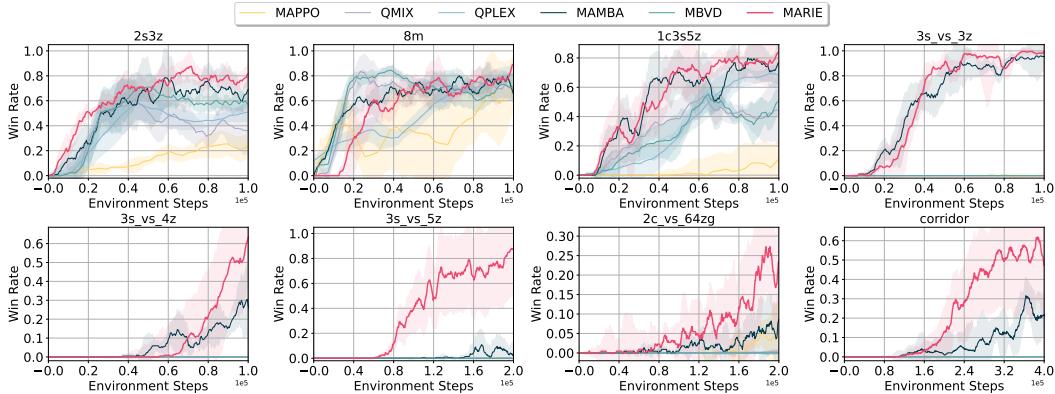


Figure 3: Curves of evaluation win rate for methods in 8 chosen SMAC maps. See Table 1 for win rates. Y axis: win rate; X axis: number of steps taken in the real environment.

Table 1: Median evaluation win rate and standard deviation on 13 SMAC maps for different methods over 4 random seeds. We bold the values of the maximum.

Maps	Difficulty	Steps	Methods					
			MARIE (Ours)	MAMBA [5]	MAPPO [49]	QMIX [35]	QPlex [46]	MBVD [48]
1c3s5z	Easy	100K	84.1 (9.4)	76.8(15.3)	22.7(11.0)	44.1(29.2)	67.2(7.4)	62.7(11.4)
2m_vs_1z			100.0 (7.9)	95.0(2.3)	86.7(3.2)	74.1(14.8)	88.4(10.8)	33.9(24.5)
2s_vs_1sc			100.0 (7.1)	99.1(7.1)	100.0(0.0)	0.0(0.0)	7.1(19.5)	0.3(14.8)
2s3z			81.8 (9.3)	69.1(12.7)	31.3(12.9)	37.7(15.5)	51.1(8.4)	52.3(4.1)
3m			99.5 (0.4)	86.4(7.1)	84.4(12.8)	53.7(22.7)	89.0(6.9)	72.4(6.9)
3s_vs_3z			99.5 (1.5)	92.3(10.1)	0.8(1.3)	0.0(0.0)	0.0(0.0)	0.0(0.0)
3s_vs_4z			63.6 (24.9)	27.7(12.3)	0.0(0.0)	0.0(0.0)	0.0(0.0)	0.0(0.0)
8m			89.1 (3.9)	65.0(7.7)	77.3(19.5)	74.5(12.8)	83.0(6.4)	74.7(9.7)
MMM			25.0(3.4)	45.0(27.6)	4.7(4.5)	25.0(17.3)	88.4 (35.1)	20.4(2.1)
so_many_baneling			97.7 (5.9)	93.6(4.1)	43.8(15.0)	22.7(8.9)	31.2(6.1)	12.6(10.4)
3s_vs_5z	Hard	200K	88.6 (38.8)	10.5(14.0)	0.0(0.0)	0.0(0.0)	0.0(0.0)	0.0(0.0)
2c_vs_64zg			23.6 (14.3)	7.7(8.7)	3.1(10.2)	0.5(0.5)	0.0(0.1)	0.0(0.4)
corridor	SuperHard	400K	47.1 (32.2)	21.1(15.2)	0.0(0.7)	0.0(0.0)	0.0(0.0)	0.0(0.0)

better policy learning within the imagination of the world model. While the scenarios become harder, e.g. *3s_vs_5z*, our world model can address the challenge of learning more intricate underlying dynamics and further large quantities of accurate imaginations, thereby significantly outperforming other baselines on these scenarios. For *MMM* where the model-free baseline performs better, we hypothesize that the agent mainly relies on short-term behaviors for cooperation, without requiring long-term predictions for better performance. Moreover, a special scenario *2c_vs_64zg* deserves attention, which features only 2 agents but with a considerably large action space of up to 70 discrete actions for each agent. It is easy for the world model to generate ridiculous estimated available action masks without understanding the mechanics behind this scenario, further leading to invalid or even erroneous policy learning in the imaginations of the world model. The performance gap on *2c_vs_64zg* proves that our Transformer-based world model has higher prediction accuracy and a deeper understanding of the underlying mechanics.

4.2 Ablation Studies

Incorporating CTDE principle with the design of the world model makes MARIE scalable and robust to different number of agents. We compare our method with a *centralized* variant of our method, wherein the world model learns the joint dynamics of all agents together over the joint trajectory $\tau = (\dots, o_t^1, o_t^2, \dots, o_t^n, a_t^1, a_t^2, \dots, a_t^n, \dots)$. Given that τ already contains the joint observations and actions, we disable the aggregation module in this *centralized* variant. As illustrated in Figure 4, our comparisons span scenarios involving 2 to 7 agents. When the number of agents is small enough, reducing the multi-agent system to a single-agent one over the joint observation and action space would not cause a prominent scalability issue, as indicated by the result in *2s_vs_1sc*. However, the scalability issue is exacerbated by a growing number of agents. In scenarios featuring more than 3 agents, the sample efficiency of the *centralized* variant encounters a significant drop, suffering from the exponential surge in spatial complexity of the joint observation-action space.

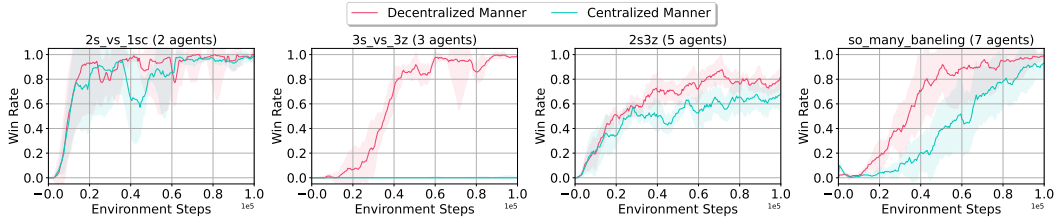


Figure 4: Ablation on what manner to integrate into the design of the world model. *Decentralized Manner* denotes the standard implementation of MARIE, while *Centralized Manner* denotes that the world model is designed for learning the joint dynamics of all agents over the joint trajectory.

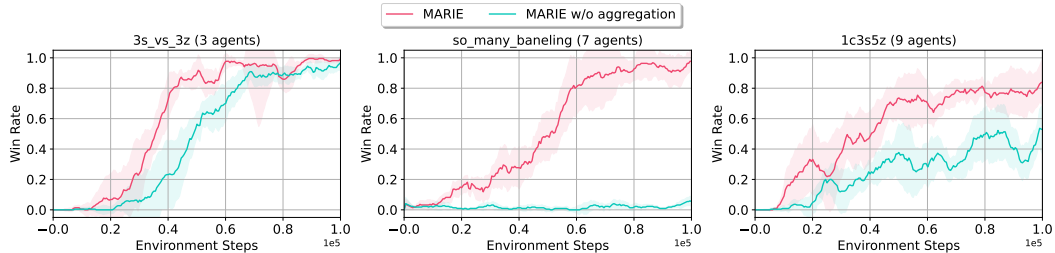


Figure 5: Comparisons between MARIE with and without the usage of the aggregation module.

Furthermore, with equal prediction horizons, the parameter amounts in the *centralized* variant is increased by a factor of 4 or larger. And to achieve the same number of environment steps, the *centralized* variant demands over twice the original computational time. Instead, with decentralized local dynamics and aggregated global features, MARIE delivers stable and superior sample efficiency.

Agent-wise aggregation helps MARIE capture the sophisticated inter-dependency on the generation of each agent’s local observation. To study the influence of agent-wise aggregation, we conduct ablation experiments on the aggregation module over scenarios where the number of agents gradually increases. As shown in Fig. 5, in the 3-agents scenario (e.g., $3s_vs_3z$), the correlation among each agent’s local observation tends to be negligible. Therefore, the nearly independent generation of each agent’s local observation without any aggregated global feature still leads to performance comparable to that of standard implementation. But as more agents get involved, the inter-dependency becomes dominant. Lacking the global features derived from agent-wise aggregation, the shared Transformer struggles to infer accurate future local observations, thus hindering policy learning in the imaginations of the world model and resulting in notable degradation in the win rate evaluation.

VQ-VAE encapsulates local observations within a succinct sequence of tokens, promoting the learning of the Transformer-based world model and effectively improving algorithm performance. Compared to VQ-VAE that discretizes each observation to K tokens from \mathcal{Z} , perhaps a more naive tokenizer is projecting the value in each dimension into one of m fixed-width bins [21], resulting in a n_{obs} -long token sequence for each observation, which we term *Bins Discretization*. We set the number of bins m equal to the size of codebook $|\mathcal{Z}|$ and compare these two types of tokenizers in different environments with various n_{obs} . As shown in Fig. 6, the performance of the two tokenizers are comparable only in $2s_vs_1sc$ where n_{obs} is close to 16. Even worse, *Bins Discretization* experiences a pronounced decline as n_{obs} increases in more complex environments (e.g., $3s_vs_4z$) under identical training durations. We hypothesize that for a single local observation, a n_{obs} -token-long verbose sequence yielded by *Bins Discretization* contains more redundant information compared to VQ-VAE that learns a more compact tokenizer through reconstruction. This not only renders the token sequences of *Bins Discretization* obscure and challenging to comprehend, but also results in an increase in model parameter amounts, being more computationally costly. Due to these two factors, *Bins Discretization* exhibits a notably slow convergence. Meanwhile, the result in $2m_vs_1z$ indicates *Bins Discretization* may ignore the correlation of different dimensions, which would be helpful in sequence modeling.

4.3 Model Analysis

Error Accumulation. A quantitative evaluation of the model’s accumulated error versus prediction horizon is provided in Fig. 7. Since learning the world model is tied to a progressively improving

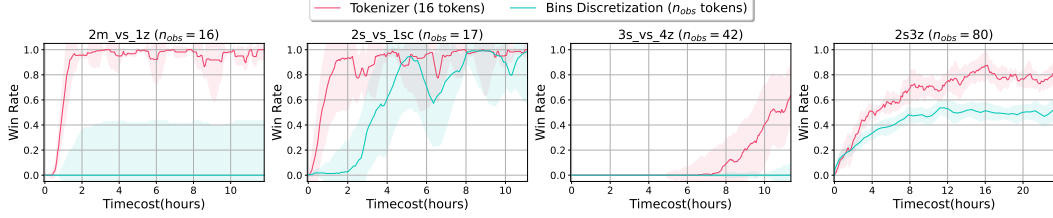


Figure 6: Ablation on the type of discretization for local observations. *Tokenizer* denotes the standard implementation of MARIE; *Bins Discretization* denotes the variant of MARIE where the n_{obs} -dimensional observation discretization is performed by projecting the value into one of m fixed-width bins in each dimension independently. X-axis: cumulative run time of algorithms in the same platform.

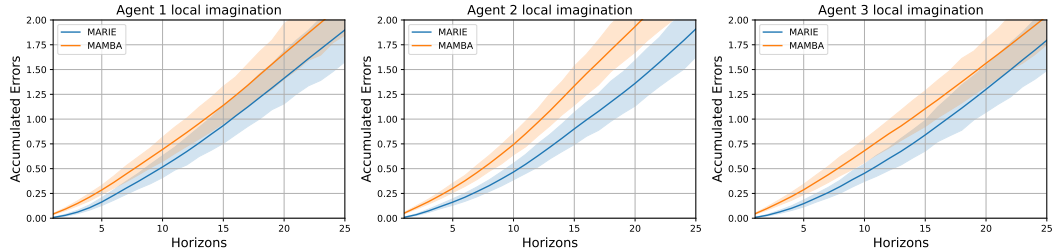


Figure 7: **Compounding model errors.** We compare the imagination accuracy of MARIE to that of MAMBA over the course of a planning horizon in $3s_vs_5z$ scenario. MARIE has remarkably better error compounding with respect to prediction horizon than MAMBA.

policy both in MARIE and MAMBA, we separately use their final policies to sample 10 episodes for fairness. We then compute L_1 errors per observation dimension between 1000 trajectory segments randomly sampled from these 20 episodes and their imagined counterpart. The result in Fig. 7 suggests architecture differences play a large role in the world model’s long-horizon accuracy. This also provides additional evidence that policy learning can benefit from accurate long-term imaginations, explaining MARIE’s notable performance in the $3s_vs_5z$ scenario. More precisely, lower generalization error between the estimated dynamics and true dynamics brings a tighter bound between optimal policies derived from these two dynamics according to theoretical results [20].

Attention Patterns. During model prediction, we delve into the attention maps inside the shared Transformer and the cross attention maps in the Perceiver. Interestingly, we observe two distinct attention patterns involved in the local dynamics prediction. One exhibits a Markovian pattern wherein the observation prediction lays its focus mostly on the previous transition, while the other is regularly striated wherein the model attends to specific tokens in multiple prior transitions. During the agent-wise aggregation, we also identify two distinct patterns – *individuality* and *commonality* among agents. Such diverse patterns in the Transformer and Perceiver may be pivotal for achieving accurate and consistent imaginations of the sophisticated local dynamics. We refer to §D for further details and visualization results.

5 Conclusion

We have introduced a model-based multi-agent algorithm – MARIE, which utilizes a shared Transformer as local dynamic model and a Perceiver as a global agent-wise aggregation module to construct a world model within the multi-agent context. By providing long-term imaginations with policy learning, it significantly boosts the sample efficiency and improves final performance compared state-of-the-art model-free methods and existing model-based methods with same learning paradigm, in the low data regime. As the first Transformer-based multi-agent world model for sample-efficient policy learning, we open a new avenue for combining the powerful strength of the Transformer with sample-efficient MARL. Considering the notorious sample inefficiency in multi-agent scenarios, it holds important promise for application in many realistic multi-robot systems, wherein collecting tremendous samples for optimal policy learning is costly and impractical due to the safety. While it has the great potential to bright the future towards achieving smarter multi-agent systems, there still

exist limitations in MARIE. For instance, it would suffer from much slower inference speed when used with a very long prediction horizons, due to the auto-regressive property.

References

- [1] Anthony Brohan, Noah Brown, Justice Carbajal, Yevgen Chebotar, Joseph Dabis, Chelsea Finn, Keerthana Gopalakrishnan, Karol Hausman, Alex Herzog, Jasmine Hsu, Julian Ibarz, Brian Ichter, Alex Irpan, Tomas Jackson, Sally Jesmonth, Nikhil Joshi, Ryan Julian, Dmitry Kalashnikov, Yuheng Kuang, Isabel Leal, Kuang-Huei Lee, Sergey Levine, Yao Lu, Utsav Malla, Deeksha Manjunath, Igor Mordatch, Ofir Nachum, Carolina Parada, Jodilyn Peralta, Emily Perez, Karl Pertsch, Jornell Quiambao, Kanishka Rao, Michael Ryoo, Grecia Salazar, Pannag Sanketi, Kevin Sayed, Jaspiar Singh, Sumedh Sontakke, Austin Stone, Clayton Tan, Hong Tran, Vincent Vanhoucke, Steve Vega, Quan Vuong, Fei Xia, Ted Xiao, Peng Xu, Sichun Xu, Tianhe Yu, and Brianna Zitkovich. Rt-1: Robotics transformer for real-world control at scale. In *Robotics: Science and Systems (RSS)*, 2023.
- [2] Tom Brown, Benjamin Mann, Nick Ryder, Melanie Subbiah, Jared D Kaplan, Prafulla Dhariwal, Arvind Neelakantan, Pranav Shyam, Girish Sastry, Amanda Askell, Sandhini Agarwal, Ariel Herbert-Voss, Gretchen Krueger, Tom Henighan, Rewon Child, Aditya Ramesh, Daniel Ziegler, Jeffrey Wu, Clemens Winter, Chris Hesse, Mark Chen, Eric Sigler, Mateusz Litwin, Scott Gray, Benjamin Chess, Jack Clark, Christopher Berner, Sam McCandlish, Alec Radford, Ilya Sutskever, and Dario Amodei. Language models are few-shot learners. In *Advances in Neural Information Processing Systems*, 2020.
- [3] Chang Chen, Yi-Fu Wu, Jaesik Yoon, and Sungjin Ahn. Transdreamer: Reinforcement learning with transformer world models. *arXiv preprint arXiv:2202.09481*, 2022.
- [4] Jacob Devlin, Ming-Wei Chang, Kenton Lee, and Kristina Toutanova. BERT: pre-training of deep bidirectional transformers for language understanding. In *Proceedings of the 2019 Conference of the North American Chapter of the Association for Computational Linguistics: Human Language Technologies, NAACL-HLT*, 2019.
- [5] Vladimir Egorov and Alexei Shpilman. Scalable multi-agent model-based reinforcement learning. In *Proceedings of the 21st International Conference on Autonomous Agents and Multiagent Systems*, 2022.
- [6] Jesse Farebrother, Jordi Orbay, Quan Vuong, Adrien Ali Taïga, Yevgen Chebotar, Ted Xiao, Alex Irpan, Sergey Levine, Pablo Samuel Castro, Aleksandra Faust, et al. Stop regressing: Training value functions via classification for scalable deep rl. *arXiv preprint arXiv:2403.03950*, 2024.
- [7] Jakob N. Foerster, Gregory Farquhar, Triantafyllos Afouras, Nantas Nardelli, and Shimon Whiteson. Counterfactual multi-agent policy gradients. In *Proceedings of the Thirty-Second AAAI Conference on Artificial Intelligence*, 2018.
- [8] David Ha and Jürgen Schmidhuber. Recurrent world models facilitate policy evolution. In *Advances in Neural Information Processing Systems*, 2018.
- [9] Danijar Hafner, Timothy Lillicrap, Jimmy Ba, and Mohammad Norouzi. Dream to control: Learning behaviors by latent imagination. In *International Conference on Learning Representations*, 2020.
- [10] Danijar Hafner, Timothy Lillicrap, Ian Fischer, Ruben Villegas, David Ha, Honglak Lee, and James Davidson. Learning latent dynamics for planning from pixels. In *Proceedings of the 36th International Conference on Machine Learning*, Proceedings of Machine Learning Research. PMLR, 2019.
- [11] Danijar Hafner, Timothy P Lillicrap, Mohammad Norouzi, and Jimmy Ba. Mastering atari with discrete world models. In *International Conference on Learning Representations*, 2021.
- [12] Danijar Hafner, Jurgis Pasukonis, Jimmy Ba, and Timothy Lillicrap. Mastering diverse domains through world models. *arXiv preprint arXiv:2301.04104*, 2023.
- [13] Nicklas Hansen, Hao Su, and Xiaolong Wang. Temporal difference learning for model predictive control. In *Proceedings of the 39th International Conference on Machine Learning*, Proceedings of Machine Learning Research. PMLR, 2022.

- [14] Nicklas Hansen, Hao Su, and Xiaolong Wang. TD-MPC2: Scalable, robust world models for continuous control. In *The Twelfth International Conference on Learning Representations*, 2024.
- [15] Dan Hendrycks and Kevin Gimpel. Gaussian error linear units (gelus). *arXiv preprint arXiv:1606.08415*, 2016.
- [16] Pablo Hernandez-Leal, Bilal Kartal, and Matthew E. Taylor. A very condensed survey and critique of multiagent deep reinforcement learning. In *Proceedings of the 19th International Conference on Autonomous Agents and MultiAgent Systems*, 2020.
- [17] Ehsan Imani and Martha White. Improving regression performance with distributional losses. In *Proceedings of the 35th International Conference on Machine Learning*, Proceedings of Machine Learning Research. PMLR, 2018.
- [18] Shariq Iqbal and Fei Sha. Actor-attention-critic for multi-agent reinforcement learning. In *Proceedings of the 36th International Conference on Machine Learning*, Proceedings of Machine Learning Research. PMLR, 2019.
- [19] Andrew Jaegle, Felix Gimeno, Andy Brock, Oriol Vinyals, Andrew Zisserman, and Joao Carreira. Perceiver: General perception with iterative attention. In *International conference on machine learning*, 2021.
- [20] Michael Janner, Justin Fu, Marvin Zhang, and Sergey Levine. When to trust your model: Model-based policy optimization. In *Advances in Neural Information Processing Systems*, 2019.
- [21] Michael Janner, Qiyang Li, and Sergey Levine. Offline reinforcement learning as one big sequence modeling problem. In *Advances in Neural Information Processing Systems*, 2021.
- [22] Andrej Karpathy. mingpt: A minimal pytorch re-implementation of the openai gpt (generative pretrained transformer) training. <https://github.com/karpathy/minGPT>, 2020.
- [23] Diederik P. Kingma and Jimmy Ba. Adam: A method for stochastic optimization. In Yoshua Bengio and Yann LeCun, editors, *3rd International Conference on Learning Representations*, 2015.
- [24] Diederik P. Kingma and Max Welling. Auto-Encoding Variational Bayes. In *2nd International Conference on Learning Representations*, 2014.
- [25] Jakub Grudzien Kuba, Ruiqing Chen, Muning Wen, Ying Wen, Fanglei Sun, Jun Wang, and Yaodong Yang. Trust region policy optimisation in multi-agent reinforcement learning. In *International Conference on Learning Representations*, 2021.
- [26] Qihan Liu, Jianing Ye, Xiaoteng Ma, Jun Yang, Bin Liang, and Chongjie Zhang. Efficient multi-agent reinforcement learning by planning. In *The Twelfth International Conference on Learning Representations*, 2024.
- [27] Yong Liu, Weixun Wang, Yujing Hu, Jianye Hao, Xingguo Chen, and Yang Gao. Multi-agent game abstraction via graph attention neural network. In *The Thirty-Fourth AAAI Conference on Artificial Intelligence*, 2020.
- [28] Ryan Lowe, Yi Wu, Aviv Tamar, Jean Harb, Pieter Abbeel, and Igor Mordatch. Multi-agent actor-critic for mixed cooperative-competitive environments. In *Proceedings of the 31st International Conference on Neural Information Processing Systems*, 2017.
- [29] Anuj Mahajan, Mikayel Samvelyan, Lei Mao, Viktor Makoviychuk, Animesh Garg, Jean Kossaiji, Shimon Whiteson, Yuke Zhu, and Animashree Anandkumar. Tesseract: Tensorised actors for multi-agent reinforcement learning. In *Proceedings of the 38th International Conference on Machine Learning*, Proceedings of Machine Learning Research. PMLR, 2021.
- [30] Vincent Micheli, Eloi Alonso, and François Fleuret. Transformers are sample-efficient world models. In *The Eleventh International Conference on Learning Representations*, 2023.
- [31] Thanh Thi Nguyen, Ngoc Duy Nguyen, and Saeid Nahavandi. Deep reinforcement learning for multiagent systems: A review of challenges, solutions, and applications. *IEEE Transactions on Cybernetics*, 50:3826–3839, 2020.
- [32] Frans A Oliehoek, Christopher Amato, et al. A concise introduction to decentralized POMDPs, volume 1. *Springer*, 2016.

- [33] Bei Peng, Tabish Rashid, Christian Schroeder de Witt, Pierre-Alexandre Kamienny, Philip Torr, Wendelin Boehmer, and Shimon Whiteson. FACMAC: Factored multi-agent centralised policy gradients. In *Advances in Neural Information Processing Systems*, 2021.
- [34] Alec Radford, Jeffrey Wu, Rewon Child, David Luan, Dario Amodei, Ilya Sutskever, et al. Language models are unsupervised multitask learners. *OpenAI blog*, 2019.
- [35] Tabish Rashid, Mikayel Samvelyan, Christian Schroeder, Gregory Farquhar, Jakob Foerster, and Shimon Whiteson. QMIX: Monotonic value function factorisation for deep multi-agent reinforcement learning. In *Proceedings of the 35th International Conference on Machine Learning*, Proceedings of Machine Learning Research. PMLR, 2018.
- [36] Jan Robine, Marc Höftmann, Tobias Uelwer, and Stefan Harmeling. Transformer-based world models are happy with 100k interactions. In *The Eleventh International Conference on Learning Representations*, 2023.
- [37] Heechang Ryu, Hayong Shin, and Jinkyoo Park. Multi-agent actor-critic with hierarchical graph attention network. In *Proceedings of the AAAI Conference on Artificial Intelligence*, 2020.
- [38] Mikayel Samvelyan, Tabish Rashid, Christian Schroeder de Witt, Gregory Farquhar, Nantas Nardelli, Tim G. J. Rudner, Chia-Man Hung, Philip H. S. Torr, Jakob Foerster, and Shimon Whiteson. The starcraft multi-agent challenge. In *Proceedings of the 18th International Conference on Autonomous Agents and MultiAgent Systems*, 2019.
- [39] Julian Schrittwieser, Ioannis Antonoglou, Thomas Hubert, Karen Simonyan, L. Sifre, Simon Schmitt, Arthur Guez, Edward Lockhart, Demis Hassabis, Thore Graepel, Timothy P. Lillicrap, and David Silver. Mastering atari, go, chess and shogi by planning with a learned model. *Nature*, 588:604 – 609, 2020.
- [40] John Schulman, Filip Wolski, Prafulla Dhariwal, Alec Radford, and Oleg Klimov. Proximal policy optimization algorithms. *arXiv preprint arXiv:1707.06347*, 2017.
- [41] Kyunghwan Son, Daewoo Kim, Wan Ju Kang, David Earl Hostallero, and Yung Yi. QTRAN: Learning to factorize with transformation for cooperative multi-agent reinforcement learning. In *Proceedings of the 36th International Conference on Machine Learning*, Proceedings of Machine Learning Research. PMLR, 2019.
- [42] Peter Sunehag, Guy Lever, Audrunas Gruslys, Wojciech Marian Czarnecki, Vinicius Zambaldi, Max Jaderberg, Marc Lanctot, Nicolas Sonnerat, Joel Z. Leibo, Karl Tuyls, and Thore Graepel. Value-decomposition networks for cooperative multi-agent learning based on team reward. In *Proceedings of the 17th International Conference on Autonomous Agents and MultiAgent Systems*, 2018.
- [43] Richard S Sutton. Dyna, an integrated architecture for learning, planning, and reacting. *ACM Sigart Bulletin*, 2(4):160–163, 1991.
- [44] Aaron van den Oord, Oriol Vinyals, and Koray Kavukcuoglu. Neural discrete representation learning. In *Advances in Neural Information Processing Systems*, 2017.
- [45] Ashish Vaswani, Noam Shazeer, Niki Parmar, Jakob Uszkoreit, Llion Jones, Aidan N Gomez, Łukasz Kaiser, and Illia Polosukhin. Attention is all you need. In *Advances in Neural Information Processing Systems*, 2017.
- [46] Jianhao Wang, Zhizhou Ren, Terry Liu, Yang Yu, and Chongjie Zhang. QPLEX: Duplex dueling multi-agent q-learning. In *International Conference on Learning Representations*, 2021.
- [47] Daniël Willemsen, Mario Coppola, and Guido CHE de Croon. Mambpo: Sample-efficient multi-robot reinforcement learning using learned world models. In *2021 IEEE/RSJ International Conference on Intelligent Robots and Systems (IROS)*. IEEE, 2021.
- [48] Zhiwei Xu, Dapeng Li, Bin Zhang, Yuan Zhan, Yunpeng Baiia, and Guoliang Fan. Mingling foresight with imagination: Model-based cooperative multi-agent reinforcement learning. In *Advances in Neural Information Processing Systems*, 2022.
- [49] Chao Yu, Akash Velu, Eugene Vinitzky, Jiaxuan Gao, Yu Wang, Alexandre Bayen, and Yi Wu. The surprising effectiveness of PPO in cooperative multi-agent games. In *Thirty-sixth Conference on Neural Information Processing Systems Datasets and Benchmarks Track*, 2022.
- [50] Qiaosheng Zhang, Chenjia Bai, Shuyue Hu, Zhen Wang, and Xuelong Li. Provably efficient information-directed sampling algorithms for multi-agent reinforcement learning. *arXiv preprint arXiv:2404.19292*, 2024.

- [51] Yang Zhang, Shixin Yang, Chenjia Bai, Fei Wu, Xiu Li, Xuelong Li, and Zhen Wang. Towards efficient llm grounding for embodied multi-agent collaboration. *arXiv preprint arXiv:2405.14314*, 2024.
- [52] Łukasz Kaiser, Mohammad Babaeizadeh, Piotr Miłoś, Błażej Osipiński, Roy H Campbell, Konrad Czechowski, Dumitru Erhan, Chelsea Finn, Piotr Kozakowski, Sergey Levine, Afroz Mohiuddin, Ryan Sepassi, George Tucker, and Henryk Michalewski. Model based reinforcement learning for atari. In *International Conference on Learning Representations*, 2020.

A World Models Details and Hyperparameters

A.1 Observation Tokenizer

Our tokenizer for local observation discretization is based on the implementation³ of a vanilla VQ-VAE [44]. Faced with continuous non-vision observation, we build the encoder and decoder as Multi-Layer Perceptrons (MLPs). The decoder is designed with the same hyperparameters as the ones of the encoder. The hyperparameters are listed as Table 2. During the phase of collecting experience from the external environment, each agent takes the reconstructed observations processed by the VQ-VAE as input instead to avoid the distribution shift between policy learning and policy execution.

For training this vanilla VQ-VAE, we use a straight-through estimator to enable gradient backpropagation through the non-differentiable quantization operation in the quantization of VQ-VAE. The loss function for learning the autoencoder is as follows:

$$\mathcal{L}_{\text{VQ-VAE}}(E, D, \mathcal{Z}) = \mathbb{E}_{i \sim \mathcal{N}} \mathbb{E}_{o^i} [\|o^i - \hat{o}^i\|^2 + \|\text{sg}[E(o^i)] - z_q^i\|^2 + \beta \|\text{sg}[z_q^i] - E(o^i)\|^2] \quad (8)$$

where $\mathcal{N} = \{1, 2, \dots, n\}$ denotes the set of agents, $\text{sg}[\cdot]$ denotes the stop-gradient operation and β is the coefficient of the commitment loss $\|\text{sg}[z_q^i] - E(o^i)\|^2$. In practice, we found the codebook \mathcal{Z} can suffer from codebook collapse when learning from scratch. Thus, we adopt the Exponential Moving Averages (EMA) [44] technique to alleviate this problem.

Table 2: VQVAE hyperparameters.

Hyperparameter	Value
Encoder&Decoder	
Layers	3
Hidden size	512
Activation	GELU[15]
Codebook	
Codebook size (N)	512
Tokens per observation (K)	16
Code dimension	128
Coef. of commitment loss (β)	10.0

A.2 Transformer

The shared Transformer serving as the local dynamics model is based on the implementation of minGPT [22]. Given a fixed imagination horizon H , it first takes a token sequence of length $H(K + 1)$ composed of observation tokens and action tokens, and embeds it into a $H(K + 1) \times D$ tensor via separate embedding tables for observations and actions. Then, the aggregated feature tensor, returned by the agent-wise aggregation module, is inserted after the action embedding tensor at every timestep, forming a final embedding tensor of shape $H(K + 2) \times D$. This tensor is forwarded through fixed Transformer blocks. Here, we adopt GPT2-like blocks [34] as the basic blocks. The hyperparameters are listed as Table 3. To enable training across all environments on a single NVIDIA RTX 3090 GPU, we adapt imagination horizon H based on the number of agents.

Table 3: Transformer hyperparameters.

Hyperparameter	Value
Imagination horizon (H)	{15, 8, 5}
Embedding dimension	256
Layers	10
Attention heads	4
Weight decay	0.01
Embedding dropout	0.1
Attention dropout	0.1
Residual dropout	0.1

³Code can be found in <https://github.com/lucidrains/vector-quantize-pytorch>

Table 4: Perceiver hyperparameters.

Hyperparameter	Value
Length of latent querying	n (number of agents)
Cross attention heads	8
Inner Transformer layers	2
Transformer attention heads	8
Dimension per attention head	64
Embedding dropout	0.1
Attention dropout	0.1
Residual dropout	0.1

A.3 Perceiver

The Perceiver [19] is based on the open-source implementation⁴. By aligning the length of the latent querying array with the number of agents n , we obtain the intrinsic global representation feature corresponding to each individual agent. We further dive into the process of agent-wise representation aggregation: (i) the embedding tensor of shape $(K + 1) \times D$ at each timestep, mentioned in Appendix A.2, is concatenated with others from all agents, thereby getting a $n(K + 1) \times D$ sequence for the joint observation-action pair at the current timestep; (ii) through the cross-attention mechanism with the latent querying array, the original sequence is compressed from length $n(K + 1)$ to n ; (iii) the compressed sequence is then forwarded through a standard transformer with bidirectional attention inside the Perceiver. The hyperparameters are listed as Table 4.

B Reward Labels in HL-Gauss

HL-Gauss method [6] leverages Histogram Losses introduced by [17]. Firstly, we can define the random variable Y with probability density f_Y and cumulative distribution function F_Y whose expectation is r_t^i . Given M buckets of width $\varsigma = (r_{\max} - r_{\min})/M$ centered at $\{b_m\}_{m=1}^M$, the distribution of Y projected onto the histogram with these buckets can be calculated via integrating over the interval $[b_m - \varsigma/2, b_m + \varsigma/2]$,

$$\begin{aligned}
 p_m(b_m) &= \int_{b_m - \varsigma/2}^{b_m + \varsigma/2} f_Y(y) dy \\
 &= F_Y(b_m + \varsigma/2) - F_Y(b_m - \varsigma/2)
 \end{aligned} \tag{9}$$

To stabilize classification learning over potential diverse reward distribution, we can model the distribution of Y as a Gaussian distribution $\mathcal{N}(\mu = r_t^i, \sigma^2)$, which smooths the target distribution computed by Eq. (9). The hyperparameter σ is used to control the degree of label smoothing, and is typically set to be 0.75ς , as advised by [6]. We refer to [6] for more details.

C Behaviour Learning Details

In MARIE, we use MAPPO-like [49] actor and critic, where the actor and critic should have been 3-layer MLPs. However, unlike other CTDE model-free approaches, whose critic takes additional global oracle states from the environment in the training phase, our world model hardly provides related predictions in the imagined trajectories. To alleviate this issue, we augment the critic with an attention mechanism and provide it all reconstructed observations \hat{o}_t of all agents. Therefore, the actor ψ remains a 3-layer MLP with ReLU activation, while the critic ξ is enhanced with an extra layer of self-attention, built on top of the original 3-layer MLP, i.e., we overwrite the critic $V_\xi^i(\hat{o}_t) \simeq \mathbb{E}_{\pi_\psi^i}(\sum_{l \geq t} \gamma^{l-t} \hat{r}_l^i)$ for agent i . Similar to off-the-shelf CTDE model-free approaches, we adopt parameter sharing across agents.

Critic loss function We utilize λ -return in Dreamer [9], which employs an exponentially-weighted average of different k -steps TD targets to balance bias and variance as the regression target for the

⁴Code can be found in <https://github.com/lucidrains/perceiver-pytorch>

Table 5: Behaviour learning hyperparameters.

Hyperparameter	Value
Imagination Horizon (H)	{15, 8, 5}
Predicted discount label γ	0.99
λ	0.95
η	0.001
Clipping parameter ϵ	0.2

critic. Given an imagined trajectory $\{\hat{o}_\tau^i, a_\tau^i, \hat{r}_\tau^i, \hat{\gamma}_\tau^i\}_{t=1}^H$ for agent i , λ -return is calculated recursively as,

$$V_\lambda^i(\hat{o}_t) = \begin{cases} \hat{r}_t^i + \hat{\gamma}_t^i \left[(1 - \lambda)V_\xi^i(\hat{o}_t) + \lambda V_\lambda^i(\hat{o}_{t+1}) \right] & \text{if } t < H \\ V_\xi^i(\hat{o}_t) & \text{if } t = H \end{cases} \quad (10)$$

The objective of the critic ξ is to minimize the mean squared difference \mathcal{L}_ξ^i with λ -returns over imagined trajectories for each agent i , as

$$\mathcal{L}_\xi^i = \mathbb{E}_{\pi_\psi^i} \left[\sum_{t=1}^{H-1} (V_\xi^i(\hat{o}_t) - \text{sg}(V_\lambda^i(\hat{o}_t)))^2 \right] \quad (11)$$

where $\text{sg}(\cdot)$ denotes the stop-gradient operation. We optimize the critic loss with respect to the critic parameters ξ using the Adam optimizer.

Actor loss function The objective for the action model $\pi_\psi(\cdot|\hat{o}_t^i)$ is to output actions that maximize the prediction of long-term future rewards made by the critic. To incorporate intermediate rewards more directly, we train the actor to maximize the same λ -return that was computed for training the critic. In terms of the non-stationarity issue in multi-agent scenarios, we adopt PPO updates, which introduce important sampling for actor learning. The actor loss function for agent i is:

$$\mathcal{L}_\psi^i = -\mathbb{E}_{p_\phi, \pi_{\psi_{\text{old}}}^i} \left[\sum_{t=0}^{H-1} \min \left(r_t^i(\psi) A_t^i, \text{clip}(r_t^i(\psi), 1 - \epsilon, 1 + \epsilon) A_t^i \right) + \eta \mathcal{H}(\pi_{\psi}^i(\cdot|\hat{o}_t^i)) \right] \quad (12)$$

where $r_t^i(\psi) = \pi_\psi^i / \pi_{\psi_{\text{old}}}^i$ is the policy ratio and $A_t^i = \text{sg}(V_\lambda^i(\hat{o}_t) - V_\xi^i(\hat{o}_t))$ is the advantage. We optimize the actor loss with respect to the actor parameters ψ using the Adam optimizer. In the discount prediction of MARIE, we set its learning target γ to be 0.99. Overall hyperparameters are shown in Table 5.

D Extended Analysis on Attention Patterns

To provide qualitative analysis of our world model, we select typical scenarios – $3s_vs_5z$ where our method achieves the most significant improvement compared to other baselines for visualizing attention maps inside the Transformer. For the sake of simple and clear visualization, we set the imagination horizon H as 5. In terms of cross-attention maps in the aggregation module, we select a scenario $2s3z$ including 5 agents for visualization. Visualization results are depicted as Fig. 8 and Fig. 9.

The prediction of local dynamics entails two distinct attention patterns. The left one in Fig. 8 can be interpreted as a Markovian pattern, in which the observation prediction lays its focus on the previous transition. In contrast, the right one is regularly striated, with the model attending to specific tokens in multiple prior observations. In terms of the agent-wise aggregation, we also identify two distinct patterns: *individuality* and *commonality*. The top one in Fig. 9 illustrates that each agent flexibly attends to different tokens according to their specific needs. In contrast, the bottom one exhibits consistent attention allocation across all agents, with attention highlighted in nearly identical positions. The diverse patterns in the Transformer and Perceiver may be the key to accurate and consistent imagination.

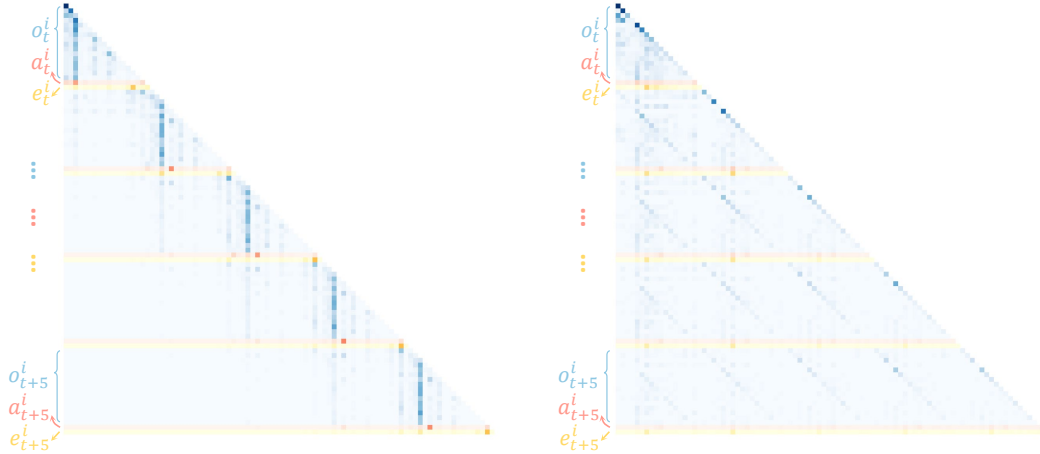


Figure 8: **Attention patterns in the Transformer.** We observe two distinct types of attention weights during the prediction of local dynamics. In the first one (*left*), the next observation prediction is primarily dependent on the last transition, which means the world model has learned the Markov property corresponding to Dec-POMDPs. The second type (*right*) exhibits a regularly striated pattern, where the next observation prediction hinges overwhelmingly on the same dimension of multiple previous timesteps. The above attention weights are produced by a sixth-layer and ninth-layer attention head during imaginations on the $3s_vs_5z$ scenario.

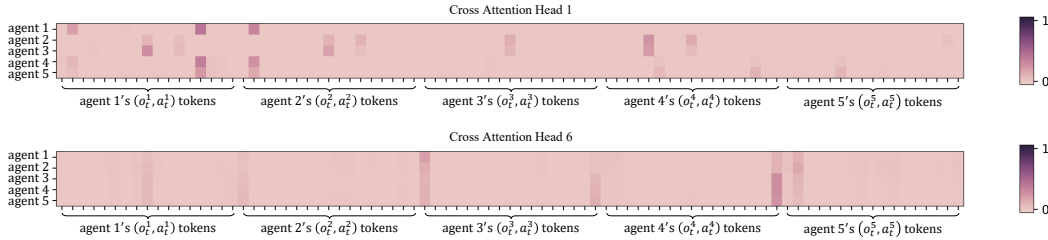


Figure 9: **Cross attention patterns in the Perceiver.** We observe the *individuality* and *commonality* in the agent-wise aggregation. The top part of the figure represents the *individuality*, where agents adjust their attentions over the whole joint token sequence at timestep t flexibly according to their own needs. In contrast, the bottom exhibits the *commonality*, where every agent’s attention over the joint token sequence is emphasized in the similar positions of the sequence. The cross attention weights mentioned above are produced by the first and sixth head of the cross attention within the Perceiver, during the agent-wise aggregation on the $2s3z$ scenario.

E Baseline Implementation Details

MAMBA [5] is evaluated based on the open-source implementation: <https://github.com/jbr-ai-labs/mamba> with the hyperparameters in Table 6.

MAPPO [49] is evaluated based on the open-source implementation: <https://github.com/marlbenchmark/on-policy> with the common hyperparameters in Table 7.

QMIX [35] is evaluated based on the open-source implementation: <https://github.com/oxwhirl/pymarl> with the hyperparameters in Table 8.

QPLEX [46] is evaluated based on the open-source implementation: <https://github.com/wjh720/QPLEX> with the hyperparameters in Table 9. Since its implementation is mostly based on the open-source implementation: PyMARL [38], its most hyperparameters setting remains the same as the one in QMIX in addition to its own special hyperparameters.

MBVD [48] is evaluated based on the implementation in its supplementary material from <https://openreview.net/forum?id=f1BYpZkWGST> with the hyperparameters in Table 10. Akin to QPLEX, its implementation is based on the open-source implementation: PyMARL, its most hyperparameters setting remains the same as the one in QMIX in addition to its own special hyperparameters.

Table 6: Hyperparameters for MAMBA in SMAC environments.

Hyperparameter	Value
Batch size	256
λ for λ -return computation	0.95
Entropy coefficient	0.001
Entropy annealing	0.99998
Number of policy updates	4
Epochs per policy update	5
Clipping parameter ϵ	0.2
Actor Learning rate	0.0005
Critic Learning rate	0.0005
Discount factor γ	0.99
Model Learning rate	0.0002
Number of model training epochs	60
Number of imagined rollouts	800
Sequence length	20
Imagination horizon H	15
Buffer size	2.5×10^5
Number of categoricals	32
Number of classes	32
KL balancing entropy weight	0.2
KL balancing cross entropy weight	0.8
Gradient clipping	100
Collected trajectories between updates	1
Hidden size	256

Table 7: Common hyperparameters for MAPPO in SMAC environments.

Hyperparameter	Value
Batch size	num envs \times buffer length \times num agents
Mini batch size	batch size / mini-batch
Recurrent data chunk length	10
GAE λ	0.95
Discount factor γ	0.99
Value loss	huber loss
Huber delta	10.0
Optimizer	Adam
Optimizer learning rate	0.0005
Optimizer epsilon	1×10^{-5}
Weight decay	0.0
Gradient clipping	10
Network initialization	orthogonal
Use reward normalization	True
Use feature normalization	True

Table 8: Hyperparameters for QMIX in SMAC environments.

Hyperparameter	Value
Batch size	32 episodes
Buffer size	5000 episodes
Epsilon in epsilon-greedy	1.0 \rightarrow 0.05
Epsilon anneal time	50000 timesteps
Train interval	1 episode
Discount factor γ	0.99
Optimizer	RMSProp
RMSProp α	0.99
RMSProp ϵ	10^{-5}
Gradient clipping	10

Table 9: Hyperparameters for QPLEX in SMAC environments.

Hyperparameter	Value
Batch size	32 episodes
Buffer size	5000 episodes
Epsilon in epsilon-greedy	1.0 \rightarrow 0.05
Epsilon anneal time	50000 timesteps
Train interval	1 episode
Discount factor γ	0.99
Optimizer	RMSProp
RMSProp α	0.99
RMSProp ϵ	10^{-5}
Gradient clipping	10
Number of layers in HyperNetwork	1
Number of heads in the attention module	4

Table 10: Hyperparameters for MBVD in SMAC environments.

Hyperparameter	Value
Batch size	32 episodes
Buffer size	5000 episodes
Epsilon in epsilon-greedy	1.0 \rightarrow 0.05
Epsilon anneal time	50000 timesteps
Train interval	1 episode
Discount factor γ	0.99
Optimizer	RMSProp
RMSProp α	0.99
RMSProp ϵ	10^{-5}
Gradient clipping	10
Number of layers in HyperNetwork	1
Number of heads in the attention module	4
Horizon of the imagined rollout	3
KL balancing α	0.3
Dimension of the latent state \hat{s}	num agents x 16

Table 11: Hyperparameters for MARIE in SMAC environments.

Hyperparameter	Value
Batch size for tokenizer training	256
Batch size for world model training	30
Optimizer for tokenizer	AdamW
Optimizer for world model	AdamW
Optimizer for actor & critic	Adam
Tokenizer learning rate	0.0003
World model learning rate	0.0001
Actor learning rate	0.0005
Critic learning rate	0.0005
Gradient clipping for actor & critic	100
Gradient clipping for tokenizer	10
Gradient clipping for world model	10
Weight decay for world model	0.01
λ for λ -return computation	0.95
Discount factor γ	0.99
Entropy coefficient	0.001
Buffer size (transitions)	2.5×10^5
Number of tokenizer training epochs	200
Number of world model training epochs	200
Collected <u>transitions</u> between updates	100 or 200
Epochs per policy update (PPO epochs)	5
PPO Clipping parameter ϵ	0.2
Number of imagined rollouts	600 or 400
Imagination horizon H	{15, 8, 5}
Number of policy updates	{4, 10, 30}
Number of stacking observations	5
Observe agent id	False
Observe last action of itself	False

F Parameters Setting in SMAC

All our experiments are run on a machine with a single NVIDIA RTX 3090 GPU, a 36-core CPU, and 128GB RAM. We provide the hyperparameters of MARIE for experiments in SMAC, shown as Table 11. To enable the running of experiments in all scenarios with a single NVIDIA RTX 3090 GPU, we set the imagination horizon H as 8 for other scenarios involving the number of agents $n > 5$, 15 for $n \leq 5$. In *so_many_baneling* and *2s3z*, we set the imagination horizon H as 5. Correspondingly, the number of policy updates in imaginations varies with imagination horizon H .

Additionally, it should be noted that the result in *3s_vs_5z* was obtained with using L1 loss function for reward prediction, which was the same as the reward prediction in MAMBA. We found the performance in this scenario is quite sensitive to the selection of reward loss function, illustrated by Fig. 10. Considering the significantly large action space of *2c_vs_64zg*, we enable the observation of agent id and last action for each agent and disable stacking the last 5 observations as input to the policy.

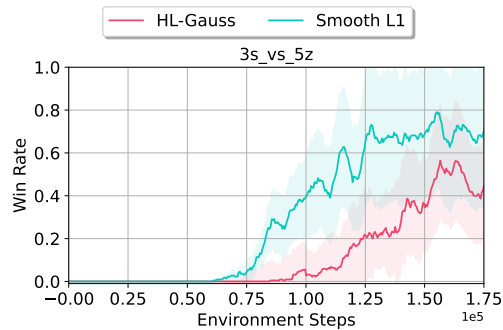


Figure 10: Performance between different loss functions for reward prediction in *3s_vs_5z*.

G Overview of MARIE Algorithm

Pseudo-code is summarized as Algorithm 1.

Algorithm 1 MARIE

```

// main loop of training
for epochs do
  collect_experience(num_transitions)
  for learning_world_model_steps_per_epoch do
    train_world_model()
  end for
  for learning_behaviour_steps_per_epoch do
    train_agents()
  end for
end for

function collect_experience(n):
   $\mathbf{o}_0 \leftarrow \text{env.reset}()$ 
  for  $t = 0, \dots, n - 1$  do
    // processed by VQ-VAE
     $\hat{\mathbf{o}}_t \leftarrow D(E(\mathbf{o}_t))$ 
    Sample  $a_t^i \sim \pi_\psi^i(a_t^i | \hat{\mathbf{o}}_t^i), \forall i$ 
     $\mathbf{o}_{t+1}, r_t, done \leftarrow \text{env.step}(\mathbf{a}_t)$ 
    if  $done = True$  then
       $\mathbf{o}_{t+1} \leftarrow \text{env.reset}()$ 
       $\gamma_t \leftarrow 0.$ 
    else
       $\gamma_t \leftarrow 0.99$ 
    end if
  end for
   $\mathcal{D} \leftarrow \mathcal{D} \cup \{\mathbf{o}_t, \mathbf{a}_t, r_t, \gamma_t\}_{t=0}^{n-1}$ 

function train_world_model():
  Sample  $\{\mathbf{o}_t, \mathbf{a}_t, r_t, \gamma_t\}_{t=\tau}^{t=\tau+H-1}$ 
  Update  $(E, D, \mathcal{Z})$  via  $\mathcal{L}_{\text{VQ-VAE}}$  over observations  $\{\mathbf{o}_t\}_{t=\tau}^{t=\tau+H-1}$ 
  for agent  $i = 1, \dots, n$  do
    Update  $\phi, \theta$  via  $\mathcal{L}_{\text{Dyn}}(\phi, \theta)$  over local trajectories  $\{\mathbf{o}_t^i, a_t^i, r_t, \gamma_t\}_{t=\tau}^{t=\tau+H-1}$ 
  end for

function train_agents():
  Sample an initial observation  $\mathbf{o}_0 \sim \mathcal{D}$ 
   $\{x_{0,j}^i\}_{j=1}^K \leftarrow E(\mathbf{o}_0^i), \hat{\mathbf{o}}_0^i \leftarrow D(E(\mathbf{o}_0^i)), \forall i$ 
  for  $t = 0, \dots, H - 1$  do
    Sample  $a_t^i \sim \pi_\psi^i(a_t^i | \hat{\mathbf{o}}_t^i), \forall i$ 
    Aggregate  $(x_{t,1}^1, \dots, x_{t,K}^1, a_t^1, \dots, x_{t,1}^n, \dots, x_{t,K}^n, a_t^n)$  into  $(e_t^1, \dots, e_t^n)$  via the Perceiver  $\theta$ 
    Sample  $\hat{x}_{t+1,\cdot}^i, \hat{r}_t^i, \hat{\gamma}_t^i \sim p_\phi(\hat{x}_{t+1,\cdot}^i, \hat{r}_t^i, \hat{\gamma}_t^i | x_{0,\cdot}^i, a_0^i, e_0^i, \dots, \hat{x}_{t,\cdot}^i, a_t^i, e_t^i), \forall i$ 
     $\hat{\mathbf{o}}_{t+1}^i \leftarrow D(\hat{x}_{t+1,\cdot}^i), \forall i$ 
  end for
  for agent  $i = 1, \dots, n$  do
    Update actor  $\pi_\psi^i$  and critic  $V_\xi^i$  via  $\mathcal{L}_{\text{Dyn}}(\phi, \theta)$  over imagined trajectories  $\{\hat{\mathbf{o}}_t^i, a_t^i, \hat{r}_t^i, \hat{\gamma}_t^i\}_{t=0}^{t=H-1}$ 
  end for

```
